

International Journal of Modern Physics E
 © World Scientific Publishing Company

Multipole expansion of densities in the deformed relativistic Hartree-Bogoliubov theory in continuum

Cong Pan

*State Key Laboratory of Nuclear Physics and Technology, School of Physics, Peking University,
 Beijing 100871, China*

Kaiyuan Zhang

*State Key Laboratory of Nuclear Physics and Technology, School of Physics, Peking University,
 Beijing 100871, China*

Shuangquan Zhang

*State Key Laboratory of Nuclear Physics and Technology, School of Physics, Peking University,
 Beijing 100871, China
 sqzhang@pku.edu.cn*

Received Day Month Year

Revised Day Month Year

The deformed relativistic Hartree-Bogoliubov theory in continuum (DRHBc) has been proved one of the best models to probe the exotic structures in deformed nuclei. In DRHBc, the potentials and densities are expressed in terms of the multipole expansion with Legendre polynomials, the dependence on which has only been touched for light nuclei so far. In this paper, taking a light nucleus ^{20}Ne and a heavy nucleus ^{242}U as examples, we investigated the dependence on the multipole expansion of the potentials and densities in DRHBc. It is shown that the total energy converges well with the expansion truncation both in the absence of and presence of the pairing correlation, either in the ground state or at a constrained quadrupole deformation. It is found that to reach a same accuracy of the total energy, even to a same relative accuracy by percent, a larger truncation is required by a heavy nucleus than a light one. The dependence of the total energy on the truncation increases with deformation. By decompositions of the neutron density distribution, it is shown that a higher-order component has a smaller contribution. With the increase of deformation, the high-order components get larger, while at the same deformation, the high-order components of a heavy nucleus play a more important role than that of a light one.

Keywords: Covariant density functional theory; deformed relativistic Hartree-Bogoliubov theory in continuum; multipole expansion; density distribution.

PACS numbers: 21.60.Jz, 21.10.Gv, 21.10.Dr

1. Introduction

The study of exotic nuclei has been one of the frontiers in both experimental and theoretical nuclear physics research.¹⁻¹⁴ Although more and more exotic nuclei are

2 *Cong Pan, Kaiyuan Zhang, Shuangquan Zhang*

experimentally produced with the development of radioactive ion beam facilities around the world,^{8,15–18} there are still a large amount of predicted nuclei far beyond the experimental capability.^{19,20} Therefore, to predict accurately the unknown properties of these nuclei, reliable microscopic theoretical methods are welcome.

The density functional theory (DFT) and its covariant version (CDFT) have provided successful descriptions for many nuclear phenomena, and have attracted wide attention in nuclear physics research.^{9–12,21–25} Based on the CDFT, the relativistic continuum Hartree-Bogoliubov (RCHB) theory considers the pairing correlation and continuum in a unified and self-consistent way,^{26,27} and has successfully provided the descriptions for many exotic nuclear phenomena.^{10,26–36} The first mass table including continuum for nuclei with $8 \leq Z \leq 120$ has recently been constructed with the RCHB theory.²⁰

Since most nuclei are deformed, Zhou and his collaborators have developed the deformed relativistic Hartree-Bogoliubov theory in continuum (DRHBc) to unifiedly describe the effects of the pairing correlation, continuum and deformation.^{37,38} The DRHBc theory has been applied to study the halo phenomena in magnesium isotopes and predicted an interesting shape decoupling between the core and the halo.^{37,38} Recently it was used to resolve the puzzles concerning the radius and configuration of valence neutrons in ^{22}C ,³⁹ and investigate the particles in the classically forbidden regions.⁴⁰ The DRHBc theory was also extended to incorporate the blocking effect in odd-nucleon systems,⁴¹ and the density-dependent meson-nucleon couplings.⁴²

In the DRHBc theory, the relativistic Hartree-Bogoliubov (RHB) equation is solved in a Dirac Woods-Saxon basis.⁴³ In addition, for axially deformed nuclei, the potentials and densities are expressed in terms of the multipole expansion with Legendre polynomials. In the existing literature, numerical checks for the DRHBc calculations, for instance, the convergence of box size and basis energy cutoff, have been carefully performed.^{38,43,44} In Ref. 38, the truncation for the Legendre expansion order was chosen as 4 for light nuclei. However, up to now there is no systematic investigation for the dependence on the Legendre expansion of the DRHBc calculations. Since nuclei may differ largely in both mass number and deformation, it is necessary to examine the convergence of the Legendre expansion for nuclei in these different cases, and find out how the DRHBc solutions depend on the high-order terms.

In this paper, a light nucleus ^{20}Ne and a heavy nucleus ^{242}U are calculated as examples to investigate the convergence of the multipole expansion with Legendre polynomials in the DRHBc theory. To study the dependence on the deformation, the constrained DRHBc calculations are performed. In Sec. 2, we give a brief theoretical framework of the DRHBc theory. The numerical details used in the calculations are given in Sec. 3. In Sec. 4 we present our results of the convergence check for the DRHBc. Finally, the work is summarized in Sec. 5.

2. Theoretical framework

The details of the DRHBc theory can be found in Refs. 37, 38 with non-linear meson exchange effective interaction, in Ref. 42 with density-dependent meson-nucleon couplings, and in Ref. 44 with point-coupling interaction. Here we only present briefly the formalism with the point-coupling interaction. By using the Bogoliubov transformation to include the pairing correlation, one can derive the RHB equation for nucleons⁴⁵

$$\begin{pmatrix} h_D - \lambda_\tau & \Delta \\ -\Delta^* & -h_D + \lambda_\tau \end{pmatrix} \begin{pmatrix} U_k \\ V_k \end{pmatrix} = E_k \begin{pmatrix} U_k \\ V_k \end{pmatrix}, \quad (1)$$

where λ_τ ($\tau = n, p$) is the chemical potential of neutron or proton, E_k and $(U_k, V_k)^T$ are the quasiparticle energy and wave function, and h_D is the Dirac Hamiltonian

$$h_D(\mathbf{r}) = \boldsymbol{\alpha} \cdot \mathbf{p} + V(\mathbf{r}) + \beta[M + S(\mathbf{r})], \quad (2)$$

with the scalar and vector potentials $S(\mathbf{r})$ and $V(\mathbf{r})$,

$$S(\mathbf{r}) = \alpha_S \rho_S + \beta_S \rho_S^2 + \gamma_S \rho_S^3 + \delta_S \Delta \rho_S, \quad (3)$$

$$V(\mathbf{r}) = \alpha_V \rho_V + \gamma_V \rho_V^3 + \delta_V \Delta \rho_V + eA_0 + \alpha_{TV} \tau_3 \rho_{TV} + \delta_{TV} \Delta \tau_3 \rho_{TV}. \quad (4)$$

Here M is the nucleon mass, and α_S , α_V , α_{TV} , β_S , γ_S , γ_V , δ_S , δ_V and δ_{TV} are the coupling constants; A_0 is the Coulomb field, and ρ_S , ρ_V and ρ_{TV} refer to the densities in scalar, vector, and isovector-vector channels, respectively.⁴⁶ The pairing potential is

$$\Delta(\mathbf{r}_1 s_1 p_1, \mathbf{r}_2 s_2 p_2) = \sum_{s'_1 p'_1} \sum_{s'_2 p'_2} V^{pp}(\mathbf{r}_1, \mathbf{r}_2; s_1 p_1, s_2 p_2; s'_1 p'_1, s'_2 p'_2) \times \kappa(\mathbf{r}_1 s'_1 p'_1, \mathbf{r}_2 s'_2 p'_2), \quad (5)$$

where s represents the spin degree of freedom, p represents the large or small component in Dirac spinor, V^{pp} is the pairing force, and κ is the pairing tensor.⁴⁷

The iterative solution of these RHB equations yields the quasiparticle levels and expectation values of total energy, quadrupole moments, etc. The total energy of a nucleus is²⁰

$$\begin{aligned} E_{\text{RHB}} = & \sum_k (\lambda_\tau - E_k) v_k^2 - E_{\text{pair}} \\ & - \int d^3 \mathbf{r} \left[\frac{1}{2} \alpha_S \rho_S^2 + \frac{1}{2} \alpha_V \rho_V^2 + \frac{1}{2} \alpha_{TV} (\rho_{TV})^2 \right. \\ & + \frac{2}{3} \beta_S \rho_S^3 + \frac{3}{4} \gamma_S \rho_S^4 + \frac{3}{4} \gamma_V (\rho_V)^4 + \frac{1}{2} \delta_S \rho_S \Delta \rho_S \\ & \left. + \frac{1}{2} \delta_V \rho_V \Delta \rho_V + \frac{1}{2} \delta_{TV} \rho_{TV} \Delta \rho_{TV} + \frac{1}{2} e A_0 \rho_p \right] \\ & + E_{\text{c.m.}}, \end{aligned} \quad (6)$$

where

$$v_k^2 = \int d^3 \mathbf{r} V_k^\dagger(\mathbf{r}) V_k(\mathbf{r}), \quad (7)$$

4 *Cong Pan, Kaiyuan Zhang, Shuangquan Zhang*

E_{pair} is the pairing energy, and $E_{\text{c.m.}}$ is the microscopic center-of-mass correction energy.^{48–50} The intrinsic quadrupole moment is calculated by

$$Q_{\tau,2} = \sqrt{\frac{16\pi}{5}} \langle r^2 Y_{20}(\theta, \phi) \rangle. \quad (8)$$

The quadrupole deformation parameter is obtained from the quadrupole moment by

$$\beta_{\tau,2} = \frac{\sqrt{5\pi} Q_{\tau,2}}{3N_{\tau} \langle r_{\tau}^2 \rangle}, \quad (9)$$

where N_{τ} refers to the number of neutron, proton, or nucleon.

In the DRHBc theory, the RHB equation (1) is solved in a Dirac Woods-Saxon basis.⁴³ For the axially deformed potentials and densities with spatial reflection symmetry in Eqs. (2), (3), (4) and (5), it is convenient to express the angular dependence in terms of the multipole expansion, where the expansion basis functions are Legendre polynomials⁵¹

$$f(\mathbf{r}) = \sum_{\lambda} f_{\lambda}(r) P_{\lambda}(\cos \theta), \quad \lambda = 0, 2, 4, \dots, \lambda_{\text{max}}, \quad (10)$$

with

$$f_{\lambda}(r) = \frac{2\lambda + 1}{4\pi} \int d\Omega f(\mathbf{r}) P_{\lambda}(\Omega), \quad (11)$$

where $f(\mathbf{r})$ refers to these potentials or densities. In practical numerical implementations, a truncation for the expansion order, λ_{max} , has to be introduced.

3. Numerical details

To investigate the convergence of the multipole expansion with Legendre polynomials in the DRHBc theory, the even-even nuclei ^{20}Ne and ^{242}U are calculated as examples. The density functional adopted is PC-PK1,⁵² which has turned out to provide one of the best density functional descriptions for nuclear masses so far.^{46,53,54} In the present convergence check against the Legendre expansion truncation λ_{max} , other numerical parameters are fixed in the DRHBc calculations. The box size is fixed at $R_{\text{max}} = 20$ fm, and the mesh size $\Delta r = 0.1$ fm. For the Woods-Saxon basis space, the angular momentum cutoff is $J_{\text{max}} = 23/2 \hbar$, and the energy cutoff is $E_{\text{cut}}^+ = 300$ MeV for positive-energy states in the Fermi sea. The number of negative-energy states in the Dirac sea is set the same as that of positive-energy states in the Fermi sea. These numerical conditions above have been examined to converge well in Refs. 43, 38, 44. When the pairing correlation is taken into account, we use the density-dependent zero-range force,^{27,38} where the pairing strength is taken as $V_0 = -325$ MeV fm³, and a sharp cutoff $E_{\text{cut}}^{\text{q.p.}} = 100$ MeV in the quasiparticle space is adopted.⁴⁴

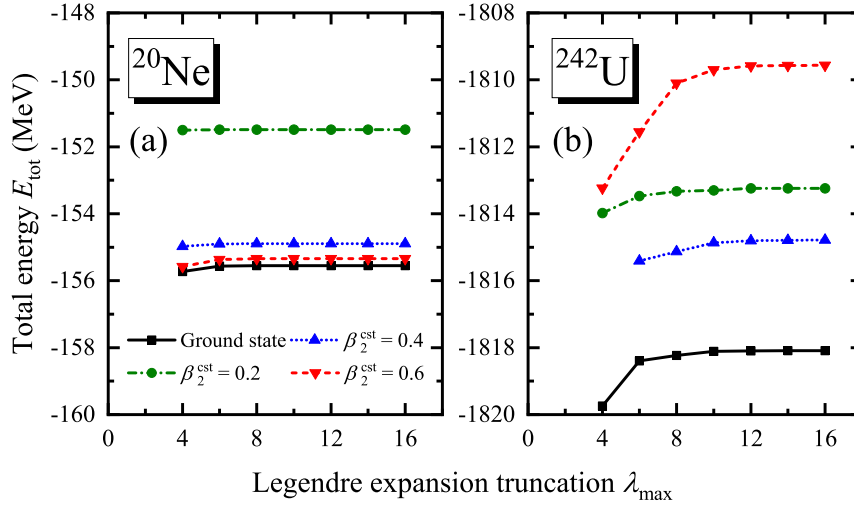


Fig. 1. Total energies of ^{20}Ne (a) and ^{242}U (b) as functions of the Legendre expansion truncation λ_{max} in the DRHBc calculations with PC-PK1. The black solid curve represents the results in the ground state, and the green dotted-dashed, blue dotted, and red dashed curves display the results with deformations constrained at $\beta_2^{\text{cst}} = 0.2, 0.4,$ and 0.6 , respectively. Here the pairing correlation is not considered.

4. Results and discussion

In Fig. 1, the total energies of a light nucleus ^{20}Ne and a heavy nucleus ^{242}U , calculated by using the DRHBc with PC-PK1, in the ground state and with deformation constrained at $\beta_2^{\text{cst}} = 0.2, 0.4$ and 0.6 , are plotted as functions of the Legendre expansion truncation λ_{max} . As a first step, in order to avoid possible coupling effects from the scattering of Cooper pairs, the pairing correlation is not considered in the calculations. As seen in Fig. 1, apparently, when λ_{max} increases, the total energies converge well in all cases considered here. For example, the deviation of the ground-state energy of ^{20}Ne is 0.178 MeV with $\lambda_{\text{max}} = 4$ from that with $\lambda_{\text{max}} = 16$, and it is 0.018 MeV with $\lambda_{\text{max}} = 6$, only about 0.01% of the total energy. In each panel, the ground state corresponds to the lowest energy, and converges to -155.548 MeV and -1818.093 MeV for ^{20}Ne and ^{242}U , respectively. It is noted that, as the ground state is obtained from the unconstrained calculation, the deformation also changes with λ_{max} . The quadrupole deformations of ^{20}Ne and ^{242}U with $\lambda_{\text{max}} = 4$ are $\beta_2 = 0.55$ and 0.32 , respectively, which converge to $\beta_2 = 0.54$ and 0.31 with $\lambda_{\text{max}} \geq 6$. Therefore, it is shown that both the total energy and deformation of the ground state converge well with λ_{max} .

To study the influence of the deformation on the convergence of λ_{max} , the results calculated at different constrained deformations are compared. In Fig. 1, the deviation of the total energy of ^{20}Ne calculated with $\lambda_{\text{max}} = 4$ from that with $\lambda_{\text{max}} = 16$ at $\beta_2^{\text{cst}} = 0.2$ is 0.016 MeV, while it is 0.081 MeV at $\beta_2^{\text{cst}} = 0.4$, and

6 *Cong Pan, Kaiyuan Zhang, Shuangquan Zhang*

0.238 MeV at $\beta_2^{\text{cst}} = 0.6$. Similarly, the deviation of the total energy of ^{242}U also increases with the constrained deformation. This shows that the dependence of the total energy on λ_{max} increases with deformation.

Then to figure out the influence of the nuclear mass on the convergence of λ_{max} , we take the largest deformation considered here, i.e. $\beta_2^{\text{cst}} = 0.6$, which poses a higher requirement for λ_{max} than others. For the light nucleus ^{20}Ne shown in Fig. 1(a), the deviations of the total energies with $\lambda_{\text{max}} = 4$ and 6 from that with $\lambda_{\text{max}} = 16$ are 0.238 MeV and 0.029 MeV, which are about 0.15% and 0.02% of the total energies, respectively, marking a good convergence. However, for the heavy nucleus ^{242}U shown in Fig. 1(b), the difference between the total energies with $\lambda_{\text{max}} = 6$ and 16 is 1.986 MeV, which is a relatively large value. By increasing λ_{max} to 8 and 10, the deviations of the total energies from that with $\lambda_{\text{max}} = 16$ are lowered to 0.534 MeV and 0.135 MeV, which are about 0.03% and 0.01% of the total energies, respectively. Therefore, to reach a same accuracy of the total energy, even to a same relative accuracy by percent, a larger λ_{max} is required for a heavy nucleus than a light one.

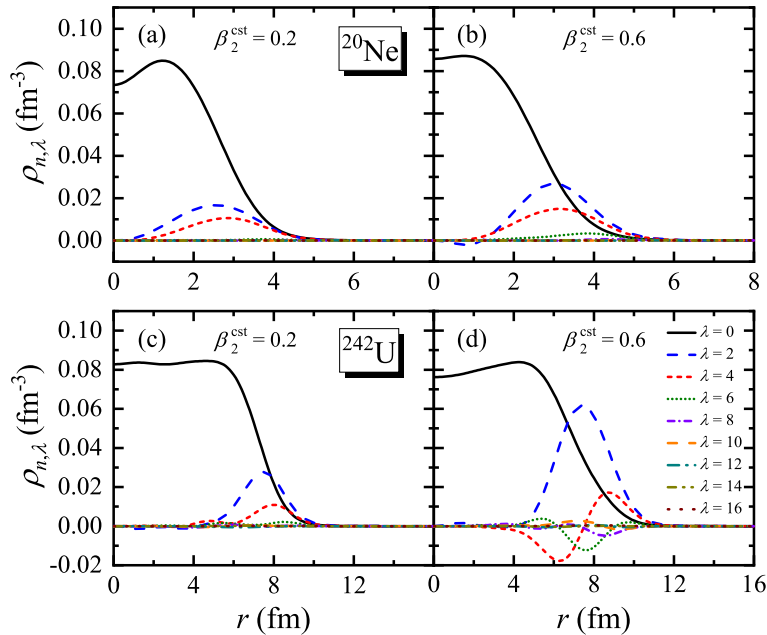


Fig. 2. Decompositions into different Legendre expansion components of the neutron densities of ^{20}Ne with deformation constrained at $\beta_2 = 0.2$ (a) and 0.6 (b), and of ^{242}U at $\beta_2 = 0.2$ (c) and 0.6 (d), in the DRHBc calculations with $\lambda_{\text{max}} = 16$.

In order to intuitively understand the behaviors of the convergence of λ_{max} shown in Fig. 1, the neutron densities ρ_n of ^{20}Ne and ^{242}U in the DRHBc calcu-

lations with $\lambda_{\max} = 16$, are both decomposed into different Legendre expansion components $\rho_{n,\lambda}$, as shown in Fig. 2. For each nucleus, the quadrupole deformation is constrained at two values, $\beta_2^{\text{cst}} = 0.2$ and 0.6 . It can be seen that in each panel of Fig. 2, the $\lambda = 0$ component $\rho_{n,0}$ is always the most important one, and with the increase of λ , the corresponding component $\rho_{n,\lambda}$ becomes smaller.

For the light nucleus ^{20}Ne , at $\beta_2^{\text{cst}} = 0.2$, as shown in Fig. 2(a), the neutron density components of $\lambda = 0 \sim 4$ are clearly seen; while at $\beta_2^{\text{cst}} = 0.6$ as shown in Fig. 2(b), it is seen that the components of $\lambda = 0 \sim 6$ are obvious, where the nonzero- λ ones are relatively larger than those at $\beta_2^{\text{cst}} = 0.2$. Therefore, with the increase of deformation, the high-order components get larger, and this is consistent with the fact that the dependence of the total energy on λ_{\max} increases with deformation. In addition, at $\beta_2^{\text{cst}} = 0.6$ the components of $\lambda > 6$ almost vanish, and this is consistent with the fact in Fig. 1(a) that the total energy of ^{20}Ne gets well converged with $\lambda_{\max} = 6$. For the heavy nucleus ^{242}U , at $\beta_2^{\text{cst}} = 0.2$, as shown in Fig. 2(c), we can clearly see the components of $\lambda = 0 \sim 4$, and also $\lambda = 6$ with small values; while at $\beta_2^{\text{cst}} = 0.6$ as shown in Fig. 2(d), the relatively obvious components are those of $\lambda = 0 \sim 8$, and $\lambda = 10$ with small values as well. This is consistent with the convergence of the total energy of ^{242}U in Fig. 1(b). Therefore, comparing Fig. 2(a) with (c), and (b) with (d), it is found at the same constrained deformation, the high-order components of a heavy nucleus play a more important role than that of a light one, which also corresponds to the influence of nuclear mass on the convergence of λ_{\max} obtained from Fig. 1.

To see more clearly and visually the spatial distributions of the different components in the Legendre expansion, in Fig. 3 the total and decomposed neutron density distributions of ^{20}Ne with deformation constrained at $\beta_2^{\text{cst}} = 0.6$ in the DRHBc calculations with $\lambda_{\max} = 16$, is plotted in x - z plane. Fig. 3(a) gives the total neutron density distribution, and the following six panels, i.e., (b) to (g), show the decompositions into different Legendre expansion components of neutron density distribution, respectively. To see the spatial distribution of high-order components more clearly, each component in panels (d) to (g) is multiplied by a factor, which can provide a reference for the order of magnitude of the corresponding density component. For $\lambda = 4, 6, 8$ and 10 , the multiplying factor is $2.5, 10, 50$, and 200 , showing that the corresponding component decreased by half a magnitude one-by-one. This is consistent with the fact in Fig. 2 that a higher λ corresponds to a smaller component $\rho_{n,\lambda}$. Furthermore, it can be seen in Fig. 3(a) that the shape of the total neutron density distribution of ^{20}Ne at $\beta_2^{\text{cst}} = 0.6$ is nearly prolate; in panel (b) the $\lambda = 0$ component is exactly spherically symmetric; and in panels (c) to (g) the components of different $\lambda \neq 0$ have the corresponding shapes with the angular part satisfying spherical harmonics $Y_{\lambda 0}$. In fact, the summation of the $\lambda = 0, 2$ and 4 components have already provided a relatively accurate description to the total density distribution in Fig. 3(a), while other components with higher λ provide higher-order corrections to the shape.

In the discussions above, the pairing correlation is neglected to avoid possible

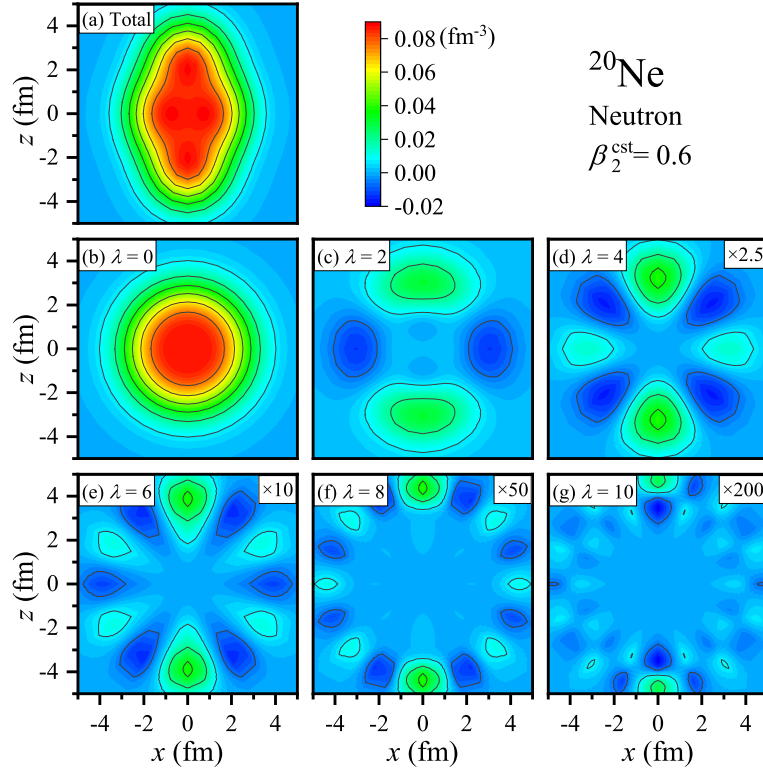
8 *Cong Pan, Kaiyuan Zhang, Shuangquan Zhang*


Fig. 3. Neutron density distributions in x - z plane of ^{20}Ne with deformation constrained at $\beta_2^{\text{cst}} = 0.6$ in the DRHBc calculations with $\lambda_{\text{max}} = 16$: (a) the total neutron density distribution, and (b) to (g) the decompositions into different Legendre expansion components of neutron density distribution, respectively. The number labeled on the upper right corner of each panel from (d) to (g) is the multiplying factor for the corresponding component.

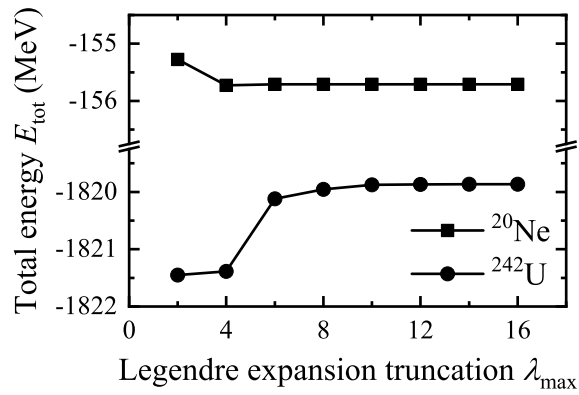


Fig. 4. Ground-state energies of ^{20}Ne and ^{242}U as functions of the Legendre expansion truncation λ_{max} in the DRHBc calculations with PC-PK1. Here the pairing correlation is included.

coupling effects from the scattering of Cooper pairs. However, in open shell nuclei, the pairing correlation plays an important role.⁴⁷ Therefore, to make it an end, it is necessary to study the convergence of the Legendre expansion truncation λ_{\max} with the pairing correlation included. Figure 4 shows the ground-state energies of ^{20}Ne and ^{242}U as functions of λ_{\max} , respectively. For ^{20}Ne the calculated ground-state energy converges to $E_{\text{tot}} = -155.708$ MeV with deformation $\beta_2 = 0.48$; for ^{242}U the corresponding results are $E_{\text{tot}} = -1819.865$ MeV with $\beta_2 = 0.30$. With the pairing correlation included, the total energy E_{tot} becomes lower and deformation β_2 smaller, as usually expected due to the pairing effects.

More explicitly, for ^{20}Ne the deviations of total energies with $\lambda_{\max} = 4$ and 6 from that with $\lambda_{\max} = 16$ are about 0.018 MeV and 0.002 MeV, respectively, which are about 0.012% and 0.002% of the total energies, whereas for ^{242}U the deviations of total energies with $\lambda_{\max} = 4, 6$ and 8 from that with $\lambda_{\max} = 16$ are about 1.521 MeV, 0.255 MeV, and 0.091 MeV, which are about 0.084%, 0.014%, and 0.005% of the total energies, respectively. Therefore, the total energy converges well, and to reach a same relative accuracy by percent, a heavy nucleus requires a higher λ_{\max} than a light one. This is similar to the results in Fig. 1, which means the inclusion of the pairing correlation does not change the conclusions from the case without the pairing correlation.

5. Summary

In summary, a light nucleus ^{20}Ne and a heavy nucleus ^{242}U have been calculated to investigate the convergence of the multipole expansion with Legendre polynomials in the deformed relativistic Hartree-Bogoliubov theory in continuum. The total energy converges well with the expansion truncation λ_{\max} both in the absence of and presence of the pairing correlation, either in the ground state or at a constrained quadrupole deformation. It is interesting to find that to reach a same accuracy of the total energy, even to a same relative accuracy by percent, a larger λ_{\max} is required for a heavy nucleus than a light one. The dependence of the total energy on λ_{\max} increases with deformation. Furthermore, by decompositions of the neutron density distribution, it is shown that its $\lambda = 0$ component is exactly spherically symmetric; and its $\lambda \neq 0$ components have the corresponding shapes with the angular part satisfying spherical harmonics $Y_{\lambda 0}$. A higher- λ component has a smaller contribution to the density distribution, and with the increase of deformation, the high-order components get larger. It is also shown at the same constrained deformation, the high-order components of a heavy nucleus play a more important role than those of a light one.

Acknowledgements

The authors would like to express gratitude to J. Meng for constructive guidance and valuable suggestions, and to J. H. Chi, Z. X. Ren, Y. K. Wang and P. W. Zhao for useful suggestions. The discussions with all members of the DRHBc mass table

10 *Cong Pan, Kaiyuan Zhang, Shuangquan Zhang*

collaboration are highly acknowledged, in particular during “the 2nd workshop on nuclear mass table with DRHBc theory”. This work was partly supported by the National Science Foundation of China (NSFC) under Grants No. 11875075, No. 11621131001, No. 11935003, and No. 11975031 and the National Key R&D Program of China (Contracts No. 2018YFA0404400 and No. 2017YFE0116700).

References

1. I. Tanihata, *Prog. Part. Nucl. Phys.* **35** (1995) 505.
2. O. Sorlin and M.-G. Porquet, *Prog. Part. Nucl. Phys.* **61** (2008) 602.
3. G. D. Alkhazov, I. S. Novikov and Y. M. Shabelski, *Int. J. Mod. Phys. E* **20** (2011) 583.
4. M. Pfützner, M. Karny, L. V. Grigorenko and K. Riisager, *Rev. Mod. Phys.* **84** (2012) 567.
5. I. Tanihata, H. Savajols and R. Kanungo, *Prog. Part. Nucl. Phys.* **68** (2013) 215.
6. D. Savran, T. Aumann and A. Zilges, *Prog. Part. Nucl. Phys.* **70** (2013) 210.
7. B. A. Brown, *Prog. Part. Nucl. Phys.* **47** (2001) 517.
8. T. Nakamura, H. Sakurai, H. Watanabe, *Prog. Part. Nucl. Phys.* **97** (2017) 53.
9. D. Vretenar, A. V. Afanasjev, G. A. Lalazissis and R. Ring, *Phys. Rep.* **409** (2005) 101.
10. J. Meng, H. Toki, S.-G. Zhou, S. Q. Zhang, W. H. Long and L. S. Geng, *Prog. Part. Nucl. Phys.* **57** (2006) 470.
11. J. Meng and S.-G. Zhou, *J. Phys. G* **42** (2015) 093101.
12. J. Meng (ed.), *Relativistic Density Functional for Nuclear Structure*, International Review of Nuclear Physics, Vol. 10 (World Scientific, Singapore, 2016).
13. S.-G. Zhou, Structure of exotic nuclei: a theoretical review, *PoS INPC 2016* (2017) 373.
14. C. Qi, R. Liotta and R. Wyss, *Prog. Part. Nucl. Phys.* **105** (2019) 214.
15. Evaluated Nuclear Structure Data File (ENSDF), <http://www.nndc.bnl.gov/ensdf>.
16. M. Thoennessen, *Rep. Prog. Phys.* **67** (2004) 1187.
17. M. Thoennessen, *Rep. Prog. Phys.* **76** (2013) 056301.
18. M. Wang, G. Audi, F. G. Kondev, W. J. Huang, S. Naimi and X. Xu, *Chin. Phys. C* **41** (2016) 030003.
19. J. Erler, N. Birge, M. Kortelainen, W. Nazarewicz, E. Olsen, A. M. Perhac and M. Stoitsov, *Nature* **486** (2012) 509.
20. X. W. Xia, Y. Lim, P. W. Zhao, H. Z. Liang, X. Y. Qu, Y. Chen, H. Liu, L. F. Zhang, S. Q. Zhang, Y. Kim and J. Meng, *At. Data Nucl. Data Tables* **121-122** (2018) 1.
21. M. Bender, P.-H. Heenen and P.-G. Reinhard, *Rev. Mod. Phys.* **75** (2003) 121.
22. P. Ring, *Prog. Part. Nucl. Phys.* **37** (1996) 193.
23. T. Nikšić, D. Vretenar and P. Ring, *Prog. Part. Nucl. Phys.* **66** (2011) 519.
24. H. Z. Liang, J. Meng and S.-G. Zhou, *Phys. Rep.* **570** (2015) 1.
25. P. W. Zhao and Z. P. Li, *Int. J. Mod. Phys. E* **27** (2018) 183007.
26. J. Meng and P. Ring, *Phys. Rev. Lett.* **77** (1996) 3963.
27. J. Meng, *Nucl. Phys. A* **635** (1998) 3.
28. J. Meng and P. Ring, *Phys. Rev. Lett.* **80** (1998) 460.
29. J. Meng, I. Tanihata and S. Yamaji, *Phys. Lett. B* **419** (1998) 1.
30. J. Meng, K. Sugawara-Tanabe, S. Yamaji, P. Ring and A. Arima, *Phys. Rev. C* **58** (1998) R628.
31. J. Meng, K. Sugawara-Tanabe, S. Yamaji and A. Arima, *Phys. Rev. C* **59** (1999) 154.

32. J. Meng, H. Toki, J. Y. Zeng, S. Q. Zhang and S.-G. Zhou, *Phys. Rev. C* **65** (2002) 041302.
33. J. Meng, S.-G. Zhou and I. Tanihata, *Phys. Lett. B* **532** (2002) 209.
34. S. Q. Zhang, J. Meng and S.-G. Zhou, *Sci. China G* **46** (2003) 632.
35. H. F. Lü, J. Meng, S. Q. Zhang and S.-G. Zhou, *Eur. Phys. J. A* **17** (2003) 19.
36. W. Zhang, J. Meng, S. Q. Zhang, L. S. Geng and H. Toki, *Nucl. Phys. A* **753** (2005) 106.
37. S.-G. Zhou, J. Meng, P. Ring and E.-G. Zhao, *Phys. Rev. C* **82** (2010) 011301.
38. L. L. Li, J. Meng, P. Ring, E.-G. Zhao and S.-G. Zhou, *Phys. Rev. C* **85** (2012) 024312.
39. X.-X. Sun, J. Zhao and S.-G. Zhou, *Phys. Lett. B* **785** (2018) 530.
40. K. Y. Zhang, D. Y. Wang and S. Q. Zhang, *Phys. Rev. C* **100** (2019) 034312.
41. L. L. Li, J. Meng, P. Ring, E.-G. Zhao and S.-G. Zhou, *Chin. Phys. Lett.* **29** (2012) 042101.
42. Y. Chen, L. L. Li, H. Z. Liang and J. Meng, *Phys. Rev. C* **85** (2012) 067301.
43. S.-G. Zhou, J. Meng and P. Ring, *Phys. Rev. C* **68** (2003) 034323.
44. K. Y. Zhang et al., *in preparation*.
45. H. Kucharek and P. Ring, *Z. Phys. A* **339** (1991) 23.
46. P. W. Zhao, L. S. Song, B. H. Sun, H. Geissel and J. Meng, *Phys. Rev. C* **86** (2012) 064324.
47. P. Ring and P. Schuck, *The Nuclear Many-Body Problem* (Springer-Verlag, 1980).
48. M. Bender, K. Rutz, P.-G. Reinhard and J. A. Maruhn, *Eur. Phys. J. A* **7** (2000) 467.
49. W. H. Long, J. Meng, N. V. Giai and S.-G. Zhou, *Phys. Rev. C* **69** (2004) 034319.
50. P. W. Zhao, B. Y. Sun and J. Meng, *Chin. Phys. Lett.* **26** (2009) 112102.
51. C. E. Price and G. E. Walker, *Phys. Rev. C* **36** (1987) 354.
52. P. W. Zhao, Z. P. Li, J. M. Yao and J. Meng, *Phys. Rev. C* **82** (2010) 054319.
53. Q. S. Zhang, Z. M. Niu, Z. P. Li, J. M. Yao and J. Meng, *Front. Phys.* **9** (2014) 529.
54. K. Q. Lu, Z. X. Li, Z. P. Li, J. M. Yao and J. Meng, *Phys. Rev. C* **91** (2015) 027304.